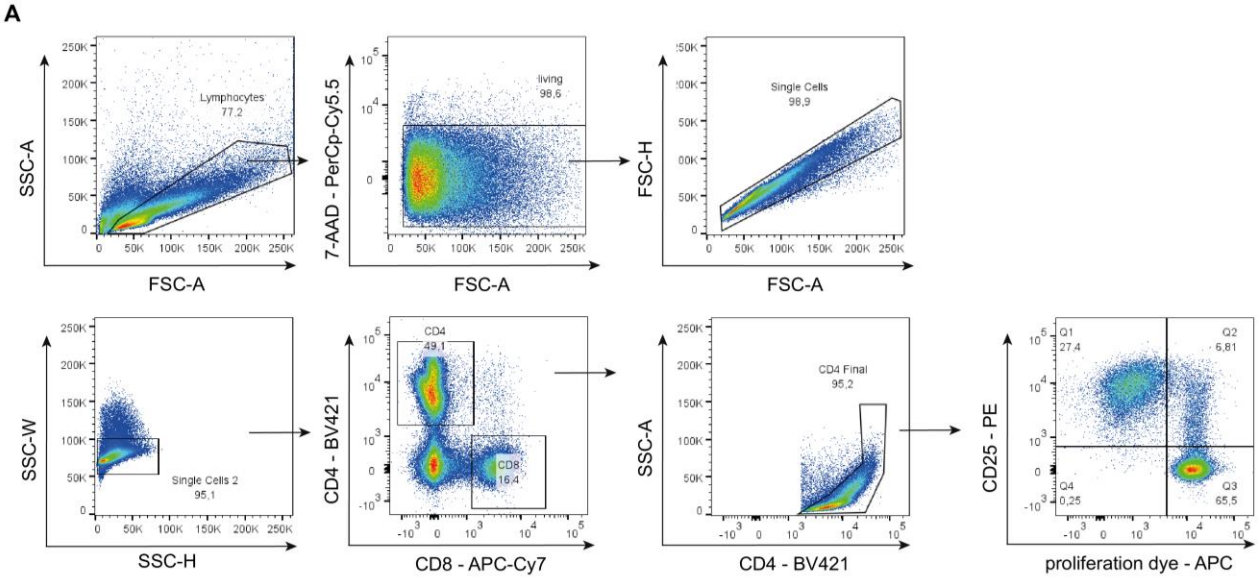
A
SSC-A
FSC-A
Lymphocytes
77,2
7-AAD - PerCp-Cy5.5
living
98,6
FSC-H
Single Cells
98,9
SSC-W
SSC-H
Single Cells 2
95,1
CD4 - BV421
CD8 - APC-Cy7
CD4
49,1
CD8
16,4
CD4 Final
95,2
CD25 - PE
proliferation dye - APC
Q1
27,4
Q2
6,81
Q4
0,25
Q3
65,5

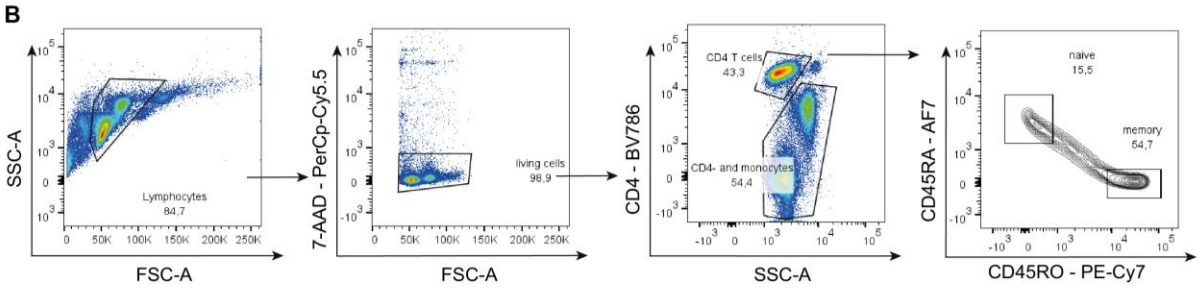
B
SSC-A
FSC-A
Lymphocytes
84,7
7-AAD - PerCp-Cy5.5
living cells
98,9
CD4 - BV786
SSC-A
CD4 T cells
43,3
CD4- and monocytes
54,4
CD45RA - AF7
CD45RO - PE-Cy7
naive
15,5
memory
54,7

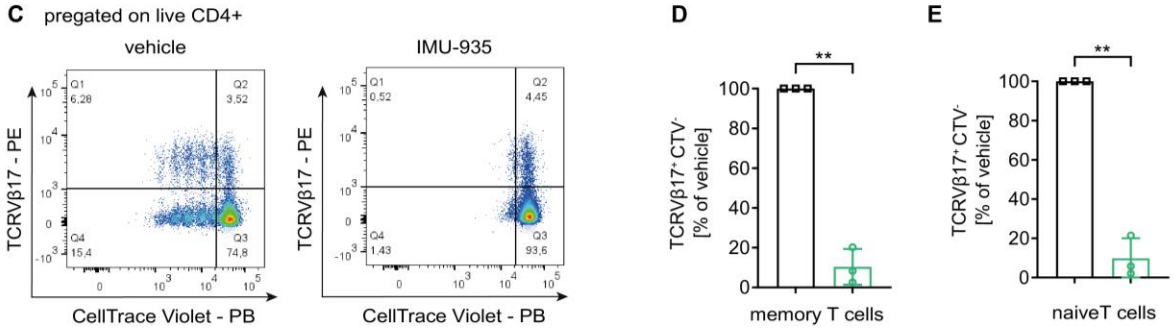
C
pregated on live CD4+
vehicle
IMU-935
TCRVβ17 - PE
CellTrace Violet - PB
Q1
6,28
Q2
3,52
Q4
15,4
Q3
74,8
Q1
0,52
Q2
4,45
Q4
1,43
Q3
93,6
D
TCRVβ17+CTV-
[% of vehicle]
memory T cells
**
E
naiveT cells
**

Fig. S1. IMU-935 reduces responses of naïve and memory CD4$^+$ T cells towards SEB antigens.

(**A**) Representative gating strategy to analyze the proliferation of human CD4$^+$ T cells in response to influenza vaccine in T cell proliferation assays.

(**B**) Representative gating strategy to sort naïve (CD45RA$^-$CD45RO$^+$), memory (CD45RA$^+$CD45RO$^-$) CD4$^+$ T cells and CD4$^+$ FACS depleted PBMC.

(**C-E**) Human T cell proliferation assay to assess TCRVβ-specific CD4$^+$ T cell response to SEB. (**C**) Representative FACS plots. Analysis of proliferating TCRVβ17$^+$CellTrace Violet CTV$^+$ CD4$^+$ T cells in response to SEB of (**D**) memory or (**E**) naïve CD4$^+$ T cells with 5nM of IMU-935 or a vehicle control, n = 3.

Each data point represents one subject. Student's t test. **=p<0.01.

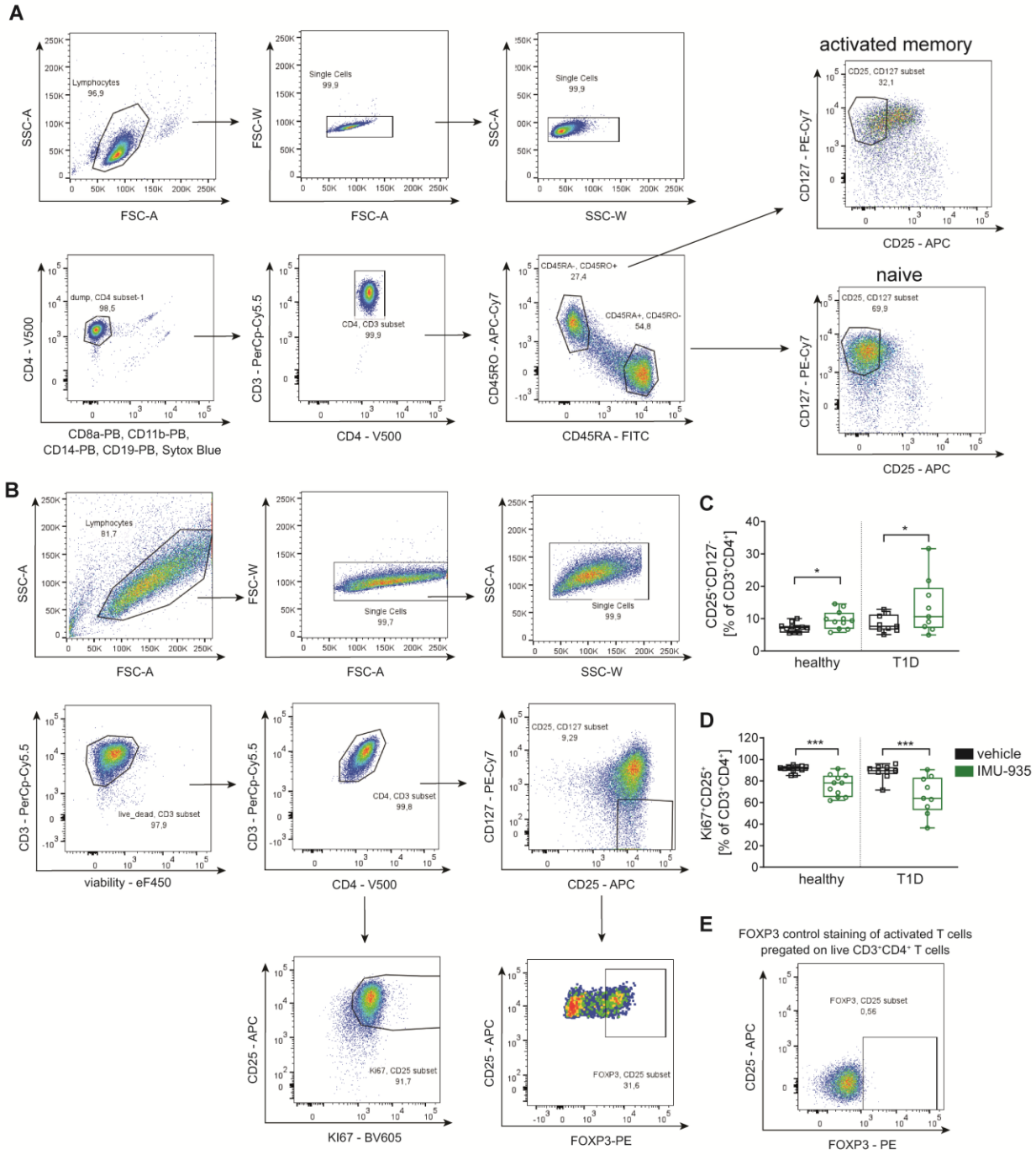
A
Lymphocytes
96,9
SSC-A
FSC-A
Single Cells
99,9
FSC-W
FSC-A
Single Cells
99,9
SSC-A
SSC-W
activated memory
CD25, CD127 subset
32,1
CD127 - PE-Cy7
CD25 - APC
dump, CD4 subset-1
98,5
CD4 - V500
CD8a-PB, CD11b-PB,
CD14-PB, CD19-PB, Sytox Blue
CD4, CD3 subset
99,9
CD3 - PerCp-Cy5.5
CD4 - V500
CD45RA-, CD45RO+
27,4
CD45RA+, CD45RO-
54,6
CD45RO - APC-Cy7
CD45RA - FITC
naive
CD25, CD127 subset
69,9
CD127 - PE-Cy7
CD25 - APC
B
Lymphocytes
81,7
SSC-A
FSC-A
Single Cells
99,7
FSC-W
FSC-A
Single Cells
99,9
SSC-A
SSC-W
live_dead, CD3 subset
97,9
CD3 - PerCp-Cy5.5
viability - eF450
CD4, CD3 subset
99,8
CD3 - PerCp-Cy5.5
CD4 - V500
CD25, CD127 subset
9,29
CD127 - PE-Cy7
CD25 - APC
KI67, CD25 subset
91,7
CD25 - APC
KI67 - BV605
FOXP3, CD25 subset
31,6
CD25 - APC
FOXP3-PE
C
CD25+CD127-
[% of CD3+CD4+]
healthy
T1D
D
KI67+CD25+
[% of CD3+CD4+]
vehicle
IMU-935
healthy
T1D
E
FOXP3 control staining of activated T cells
pregated on live CD3+CD4+ T cells
FOXP3, CD25 subset
0,56
CD25 - APC
FOXP3 - PE
F
IL-10+
[% of CD25+CD127-FOXP3+]
0.12
healthy
T1D
G
IFNγ+
[% of CD25+CD127-FOXP3+]
0.31
healthy
T1D
H
LAG3+
[% of CD25+CD127-FOXP3+]
0.12
healthy
T1D

Fig. S2. IMU-935 enhances $CD25^{+}CD127^{-}$ Tregs in human Treg induction *in vitro*.

(**A**) Representative gating strategy for human naïve and previously activated memory T cells.

(**B**) Representative FACS plots for the analysis of human Treg induction *in vitro*.

(**C, D**) Human Treg induction *in vitro* using subimmunogenic TCR stimulation and naïve T cells isolated from PBMCs of healthy subjects or T1D donors in presence or absence of 3.5 nM IMU-935. Summary plots for the frequency of (**C**) induced $CD25^{+}CD127^{-}$ $CD3^{+}CD4^{+}$ Tregs and (**D**) proliferating $CD25^{+}Ki67^{+}CD3^{+}CD4^{+}$ T cells. Healthy n = 10, T1D n = 9.

(**E**) Representative FACS plots of FOXP3 staining among sorted activated human T cells, pregated on $CD3^{+}CD4^{+}$ T cells.

(**F-H**) Human Treg induction *in vitro* using continuous TCR stimulation and naïve T cells isolated from PBMCs of healthy subjects or T1D donors in presence or absence of 1 µM IMU-935. Summary plots for the frequency of (**F**) $IL\text{-}10^{+}$ producing cells, (**G**) $IFN\gamma^{+}$ producing cells and (**H**) $LAG3^{+}$ expressing cells of induced $CD25^{+}CD127^{-}FOXP3^{+}$ Tregs. Healthy n = 3, T1D n = 3. Each data point represents one subject, experiments were performed in 2-3 technical replicates. Student's *t* test. *=p<0.05; ***=p<0.001.

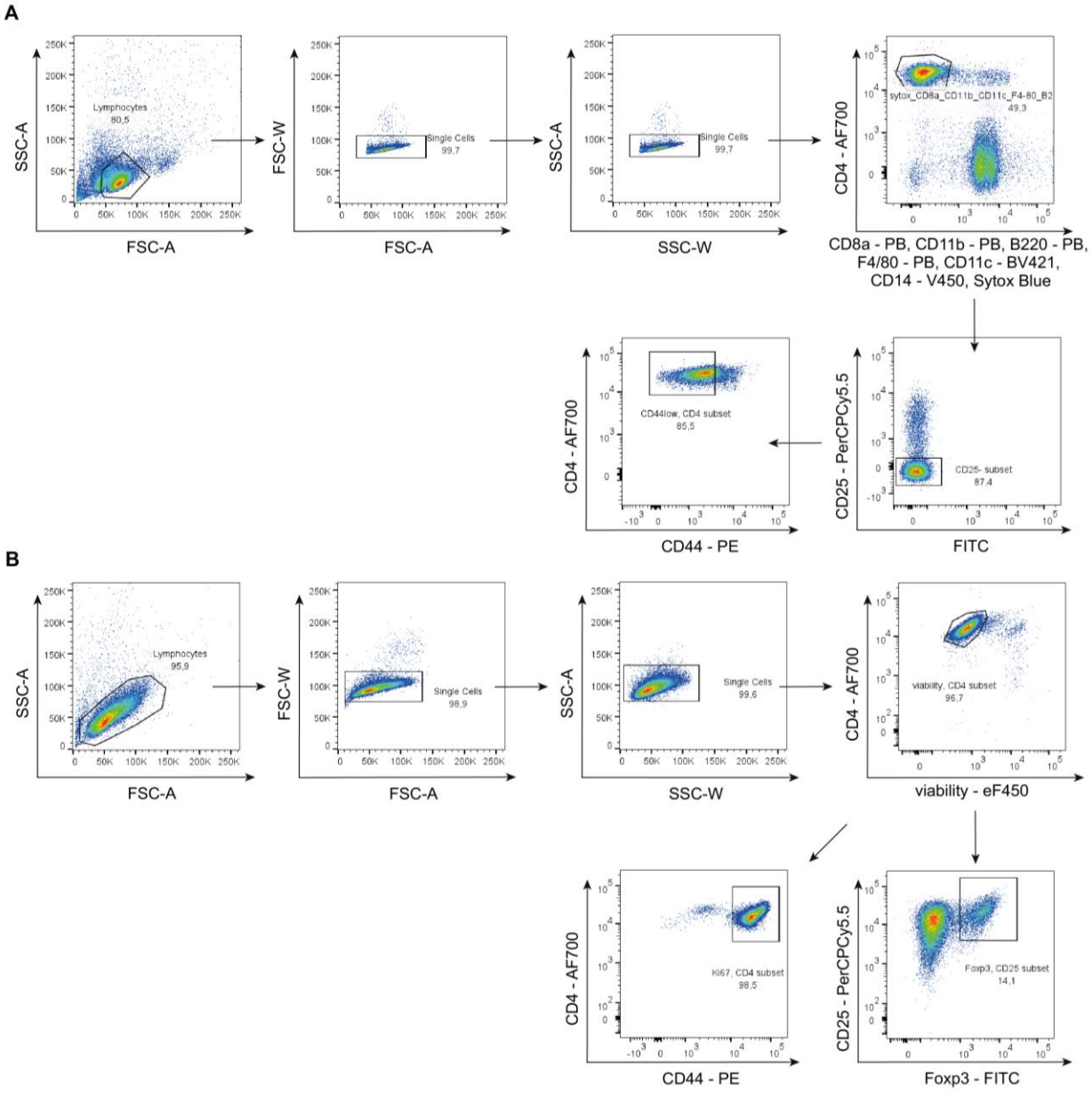

C pregated with doublet cell exclusion

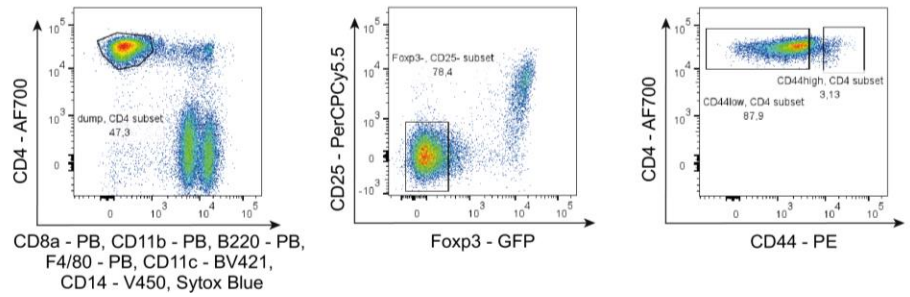

Fig. S3. Gating strategy for FACS sorting and analysis of murine T cells.

(**A**) Representative FACS plots for the sort of murine naïve T cells.

(**B**) Representative FACS plots for the analysis of $CD25^{+}Foxp3^{+}$ Tregs and $Ki67^{+}$ T cells after Treg induction *in vitro*.

(**C**) Representative FACS plots for the sort of naïve and activated T cells from $Foxp3^{GFP}$ Balb/c mice.

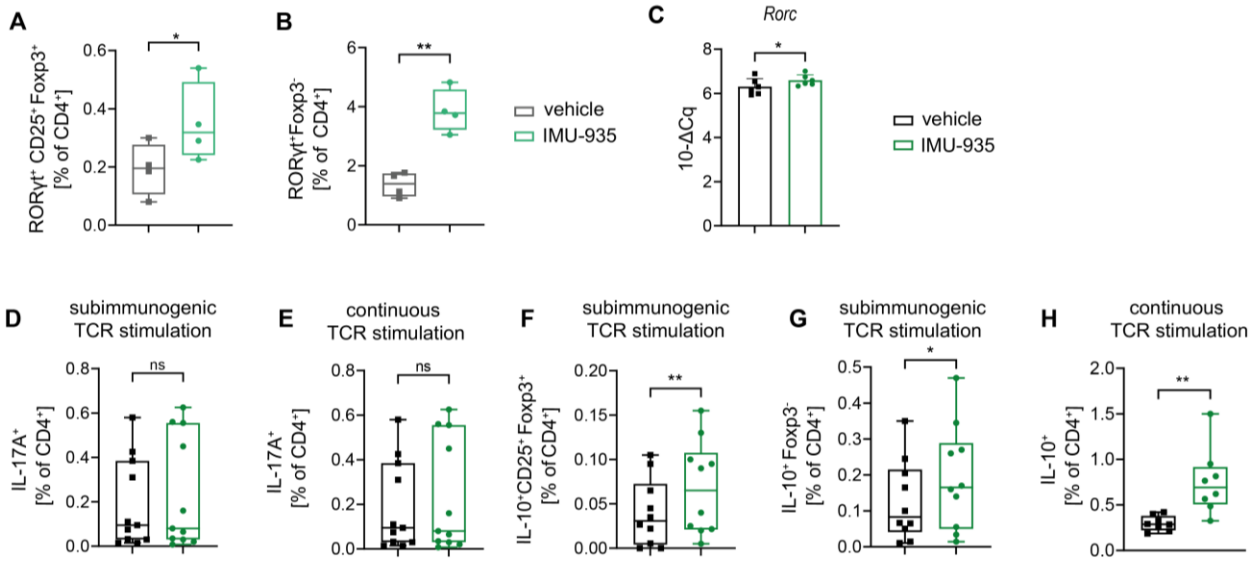

Fig. S4. IMU-935 enhances RORγt expression while fostering an anti-inflammatory phenotype after Treg induction *in vitro*.

(**A, B**) Murine Treg induction *in vitro* using subimmunogenic TCR stimulation and naïve T cells from LN of RORγt^{GFP}Foxp3^{RFP} reporter mice in presence of 1 µM IMU-935 or the vehicle control. Summary plot for (**A**) RORγt^{+}CD25^{+}Foxp3^{+} Tregs and (**B**) RORγt^{+}Foxp3^{-} T cells, n = 4.

(**C**) qPCR analysis of *Rorc* gene expression of sorted live CD4^{+} T cells after Treg induction *in vitro* using continuous TCR stimulation and naïve T cells isolated from LN of NOD mice in presence or absence of IMU-935. Gene expression was normalized to *Histone H3*, n = 6.

(**D, E**) Frequency of IL-17^{+} T cells after Treg induction *in vitro* using naïve T cells isolated from LN of NOD mice and (**D**) subimmunogenic (n = 11) or (**E**) continuous TCR stimulation (n = 7) in presence of 1 µM IMU-935 or the vehicle control.

(**F**) Frequency of IL10^{+}CD25^{+}Foxp3^{+} Tregs and (**G**) IL10^{+}Foxp3^{-} T cells after Treg induction *in vitro* using subimmunogenic TCR stimulation and naïve T cells isolated from LN of NOD mice in presence of 1µM IMU-935 or the vehicle control, n = 10.

(**H**) Frequency of IL10^{+} cells among all live CD4^{+} T cells after Treg induction *in vitro* using continuous TCR stimulation and naïve T cells isolated from LN of NOD mice in presence of 1 µM IMU-935 or the vehicle control, n = 8.

Each data point represents one subject, experiments were performed in 2-3 technical replicates. Student's t test. *=p<0.05; **=p<0.01; ***=p<0.001.

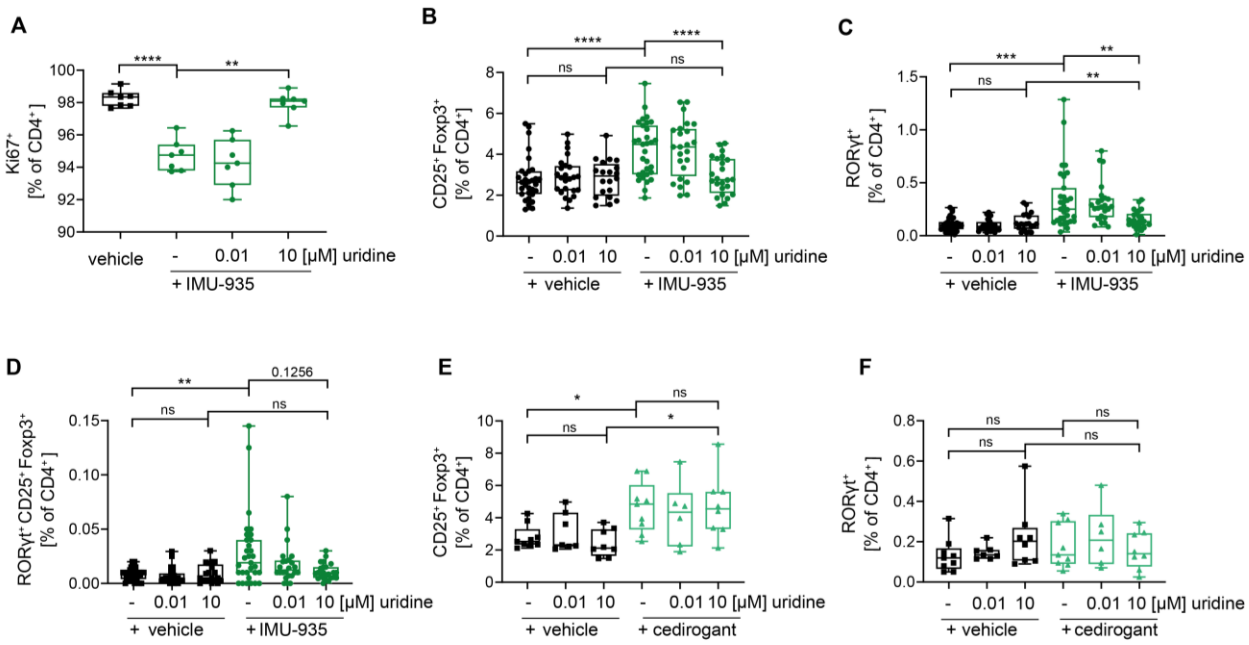

Fig. S5. Excess of uridine diminishes effects of IMU-935 on Treg induction *in vitro*.

(**A**) Frequency of proliferating Ki67$^+$ T cells after murine subimmunogenic Treg induction *in vitro* using naïve T cells isolated from LN of NOD mice in presence or absence of 1 μM IMU-935 and increasing concentrations of uridine, n = 7.

(**B-D**) *In vitro* Treg induction in the presence of the proinflammatory cytokines IL-6, IFN-γ and IL-1β and using naïve T cells isolated from LN of NOD mice with or without 1 μM IMU-935 and increasing concentrations of uridine. Summary plots for the frequency of (**B**) CD25$^+$Foxp3$^+$ Tregs (**C**) RORγt$^+$ T cells and (**D**) Rorγt$^+$CD25$^+$Foxp3$^+$ Tregs, n = 20-31.

(**E, F**) *In vitro* Treg induction in the presence of the proinflammatory cytokines IL-6, IFN-γ and IL-1β using naïve T cells isolated from LN of NOD mice with or without the RORγt inverse agonist cedirogant (10 μM) and increasing concentrations of uridine. Frequency of (**E**) CD25$^+$Foxp3$^+$ Tregs and (**F**) RORγt$^+$ T cells, n = 6-9.

Each data point represents one subject, experiments were performed in 2-3 technical replicates. One-way ANOVA with Tukey's post hoc test for multiple comparisons. *=p<0.05; **=p<0.01; ***=p<0.001; ****=p<0.0001.

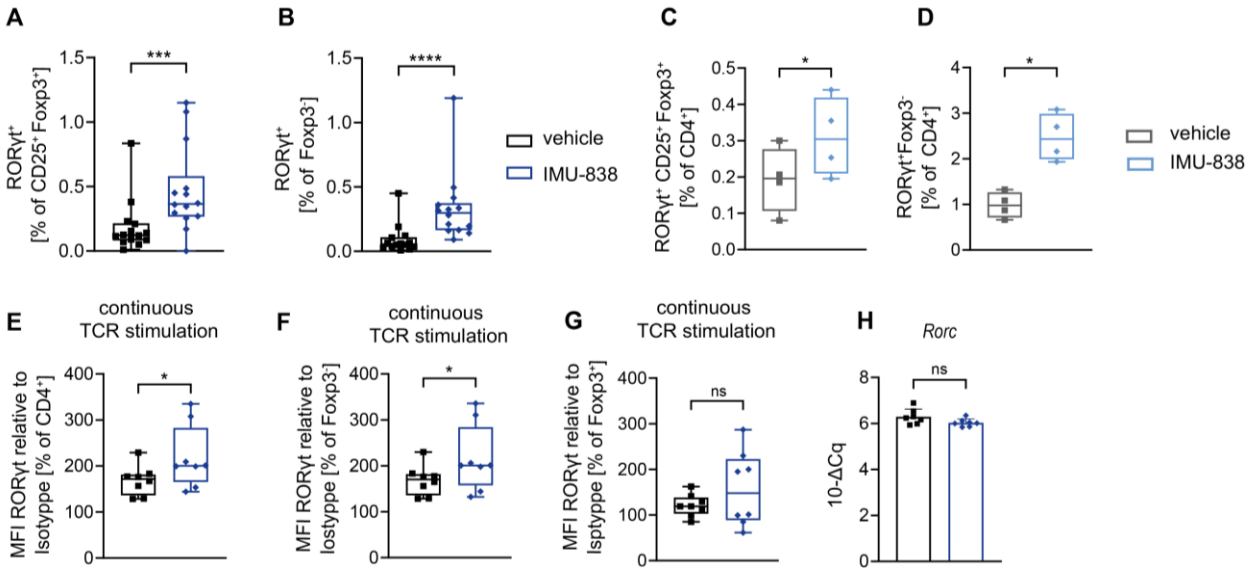

Fig. S6. IMU-838 enhances RORγt⁺ Treg and non-Treg frequency after Treg induction *in vitro*.

(**A, B**) Frequency of RORγt in (**A**) CD25⁺Foxp3⁺ Tregs or (**B**) Foxp3⁻ non-Tregs after Treg induction *in vitro* using subimmunogenic TCR stimulation and naïve T cells from LN of NOD mice in presence or absence of 50 µM IMU-838, n = 14.

(**C, D**) Frequency of (**C**) RORγt⁺CD25⁺Foxp3⁺ Tregs or (**D**) RORγt⁺Foxp3⁻ non-Tregs after Treg induction *in vitro* using subimmunogenic TCR stimulation and naïve T cells from LN of RORγt^{GFP}Foxp3^{RFP} reporter mice in presence or absence of 50 µM IMU-838, n = 4.

(**E-G**) Isotype-normalized MFI of RORγt in (**E**) total CD4⁺ T cells, (**F**) Foxp3⁻ non-Tregs and (**G**) CD25⁺Foxp3⁺ Tregs after Treg induction *in vitro* using continuous TCR stimulation and naïve T cells from LN of NOD mice in presence or absence of 50 µM IMU-838, n = 8.

(**H**) qPCR analysis of *Rorc* gene expression of sorted live CD4⁺ T cells after Treg induction *in vitro* using continuous TCR stimulation and naïve T cells isolated from LN of NOD mice in presence or absence of 50 µM IMU-838. Gene expression was normalized to *Histone H3*, n = 7.

Each data point represents one subject, experiments were performed in 2-3 technical replicates. Student's *t* test. *=p<0.05; ***=p<0.001; ****=p<0.0001.

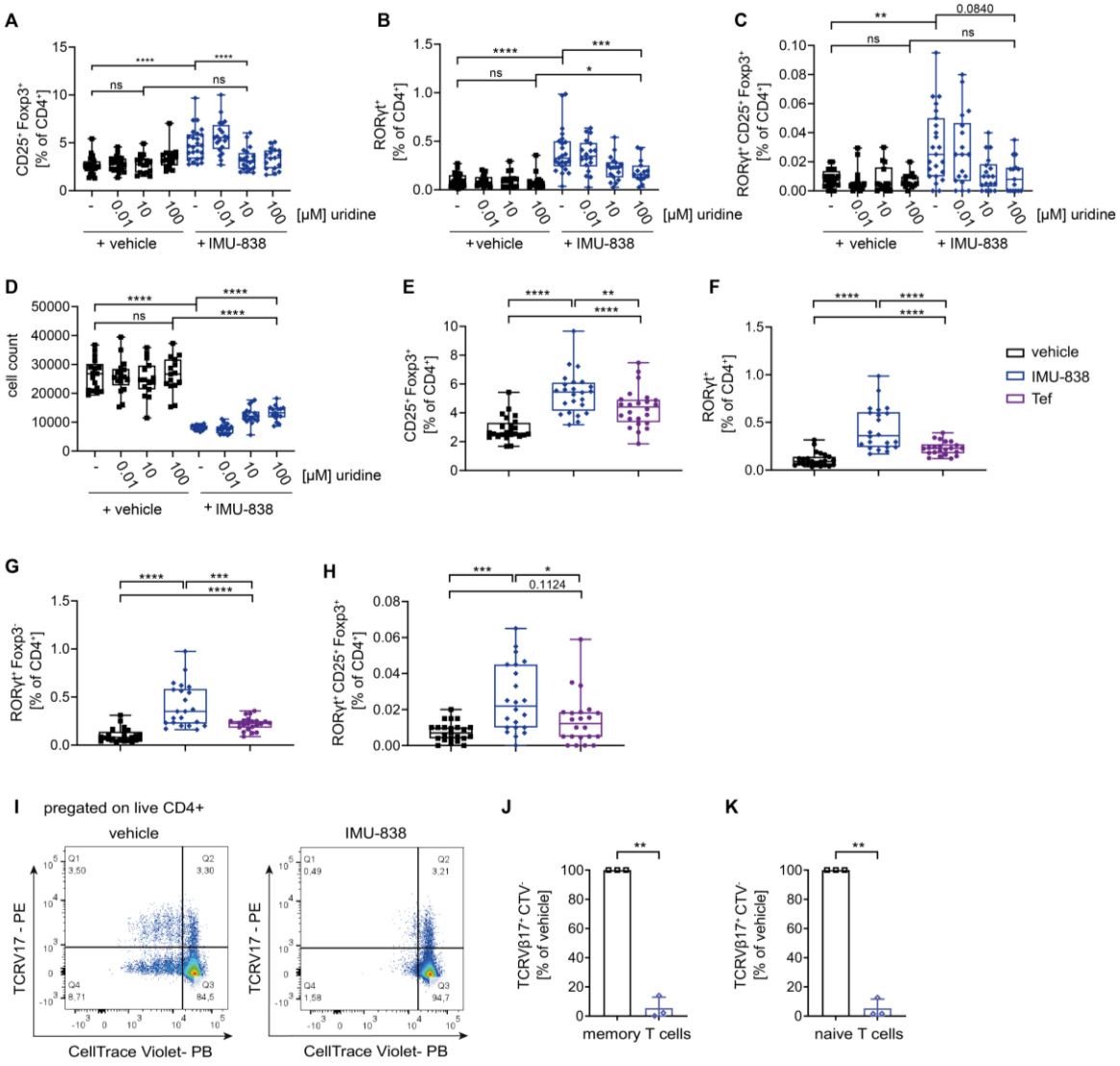

Fig. S7. DHODH inhibition enhances murine Treg induction *in vitro*.

(**A-D**) *In vitro* Treg induction in the presence of the proinflammatory cytokines IL-6, IFN-γ and IL-1β and using naïve T cells isolated from LN of NOD mice with or without 50 μM IMU-838 and increasing concentrations of uridine. Summary plots for the frequency of (**A**) CD25$^+$Foxp3$^+$ Tregs (**B**) RORγt$^+$ T cells (**C**) Rorγt$^+$CD25$^+$Foxp3$^+$ Tregs (**D**) cell count of total recovered cells, n = 14-26 experiments with 2-3 technical replicates.

(**E-H**) Frequency of (**E**) CD25$^+$Foxp3$^+$ Tregs, (**F**) RORγt$^+$ T cells, (**G**) RORγt$^+$Foxp3$^-$ non-Tregs and (**H**) RORγt$^+$CD25$^+$Foxp3$^+$ Tregs after Treg induction *in vitro* in the presence of the proinflammatory cytokines IL-6, IFN-γ and IL-1β and using naïve T cells isolated from

LN of NOD mice with or without 50 µM IMU-838 or 7.5 µM Teriflunomide (Tef), n = 22-24 experiments with 2-3 technical replicates.

(**I-K**) Human T cell proliferation assay to assess TCRVβ-specific $CD4^+$ T cell response to SEB. (**I**) Representative FACS plots. Analysis of proliferating $TCRV\beta17^+$CellTrace Violet CTV^+ $CD4^+$ T cells in response to SEB of (**J**) memory or (**K**) naïve $CD4^+$ T cells with 10 µM of IMU-838 or a vehicle control, n = 3. Each data point represents one subject, (A-H) experiments were performed in 2-3 technical replicates. (A-H) One-way ANOVA with Tukey's post hoc test for multiple comparisons, (J, K) Student's t-test. *=p<0.05; **=p<0.01; ***=p<0.001; ****=p<0.0001.

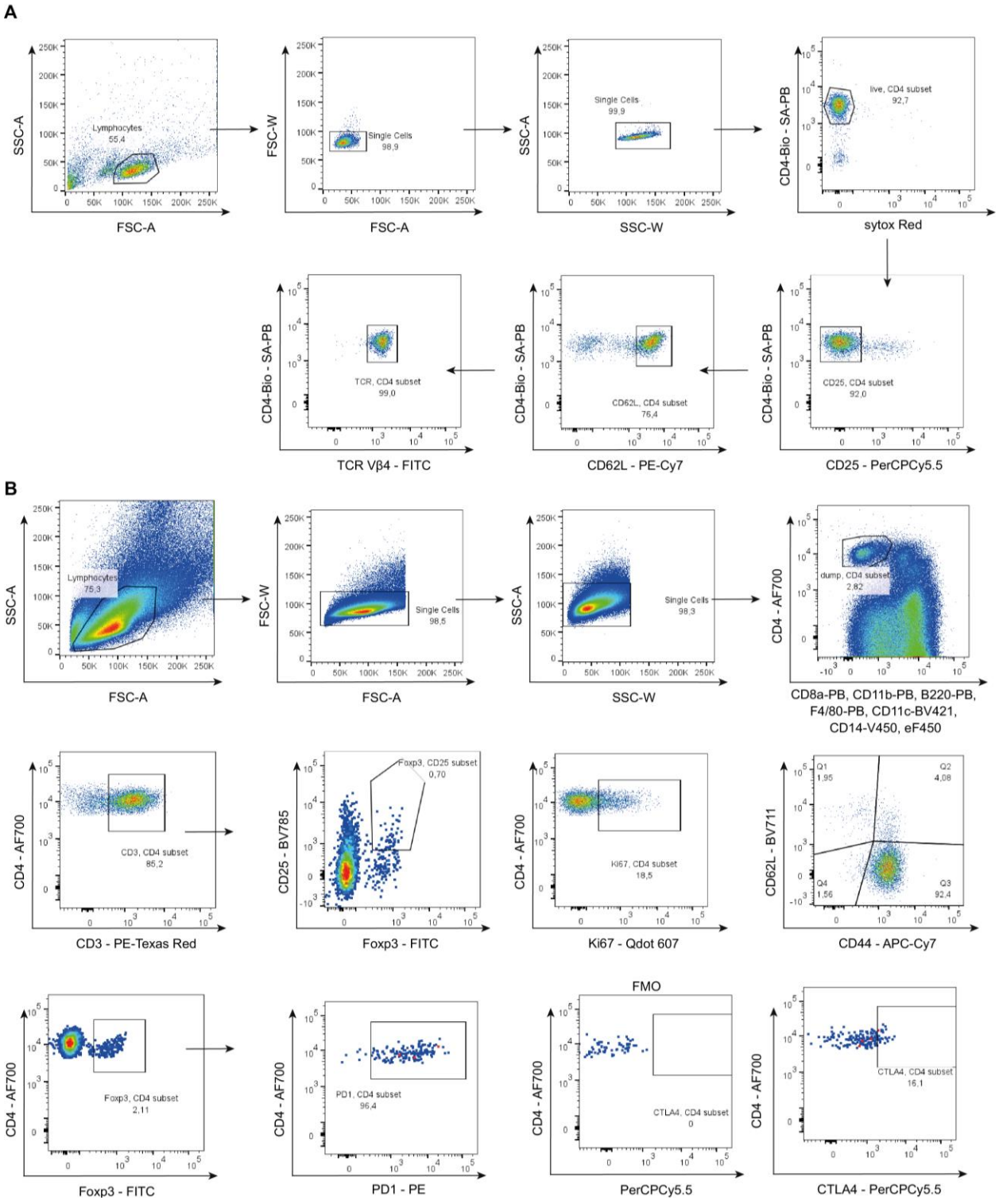
A
SSC-A
FSC-A
Lymphocytes
55,4
FSC-W
Single Cells
98,9
SSC-W
Single Cells
99,9
CD4-Bio - SA-PB
sytox Red
live, CD4 subset
92,7
CD25 - PerCPCy5.5
CD25, CD4 subset
92,0
CD62L - PE-Cy7
CD62L, CD4 subset
76,4
TCR Vβ4 - FITC
TCR, CD4 subset
99,0
B
Lymphocytes
75,3
Single Cells
98,5
Single Cells
98,3
CD4 - AF700
dump, CD4 subset
2,82
CD8a-PB, CD11b-PB, B220-PB,
F4/80-PB, CD11c-BV421,
CD14-V450, eF450
CD3 - PE-Texas Red
CD3, CD4 subset
85,2
CD25 - BV785
Foxp3 - FITC
Foxp3, CD25 subset
0,70
Ki67 - Qdot 607
Ki67, CD4 subset
18,5
CD62L - BV711
CD44 - APC-Cy7
Q1
1,95
Q2
4,08
Q4
1,56
Q3
92,4
Foxp3 - FITC
Foxp3, CD4 subset
2,11
PD1 - PE
PD1, CD4 subset
96,4
FMO
PerCPCy5.5
CTLA4, CD4 subset
0
CTLA4 - PerCPCy5.5
CTLA4, CD4 subset
16,1

Fig. S8. Analysis of IMU-838 treatment in a T1D mouse model induced by adoptive transfer.

(**A**) Representative gating strategy for the FACS sort of live $CD4^+CD25^-CD62L^+TCRV\beta4^+$ T cells from NOD BDC2.5 mice.

(**B**) Representative FACS plots for the gating strategy for the analysis from Fig. 5.

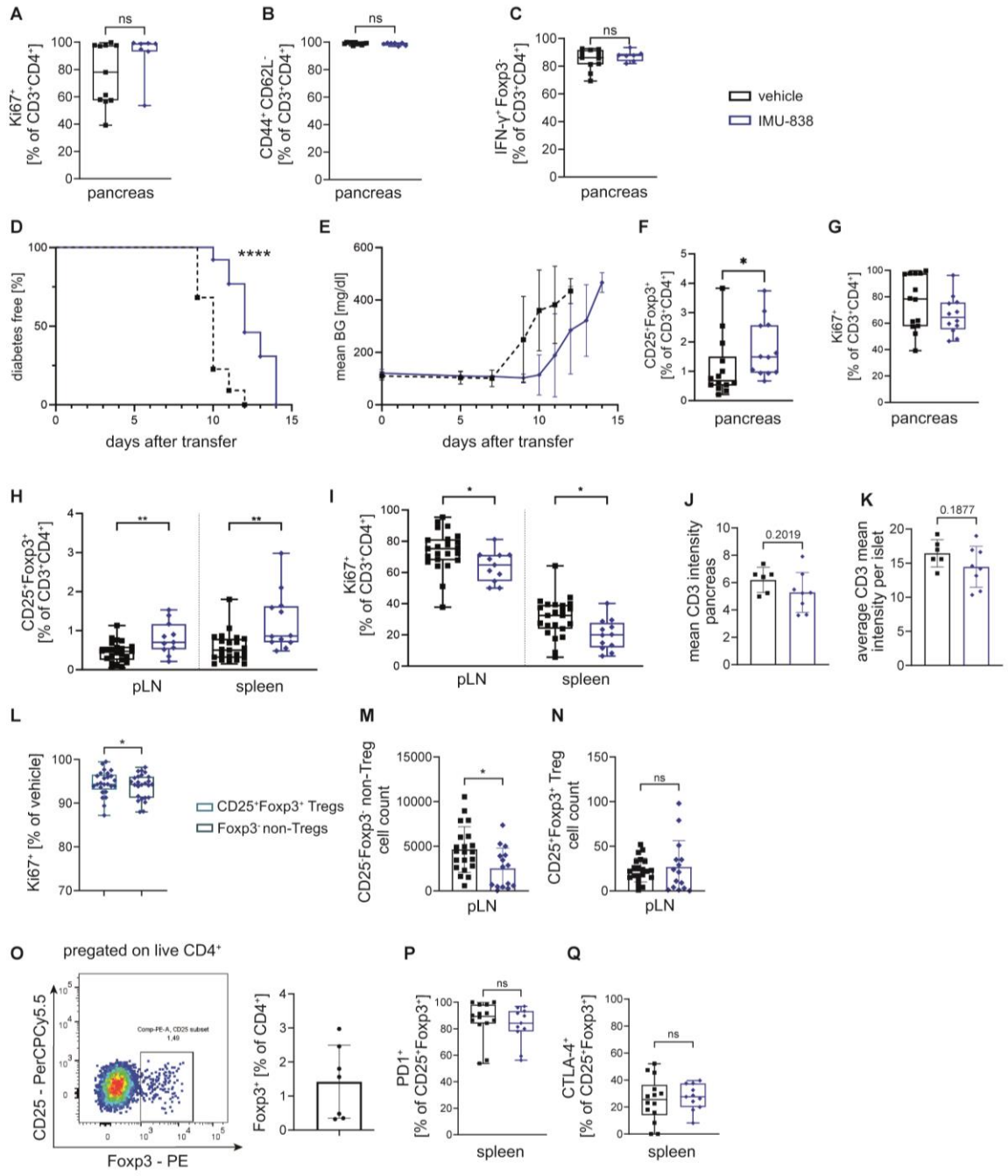

Fig. S9. Impact of IMU-838 treatment in a mouse model of accelerated T1D.

(**A-C**) Frequency of (**A**) proliferating Ki67$^+$CD3$^+$CD4$^+$ T cells, (**B**) activated CD44$^+$CD62L$^-$ CD3$^+$CD4$^+$ T cells and (**C**) IFNγ$^+$CD3$^+$CD4$^+$ T cells in the pancreas in mice treated with the vehicle control or IMU-838 in the mouse model of accelerated T1D, vehicle n = 11, IMU-838 n = 7.

(**D**) Follow up incidence study in the mouse model of accelerated T1D, vehicle n=22, IMU-838 n=13.

(**E**) Mean blood glucose values of the mice in D.

(**F, G**) Frequencies of (**F**) $CD25^+Foxp3^+$ T cells and (**G**) proliferating $Ki67^+CD3^+CD4^+$ T cells in the pancreas of mice treated with the vehicle control or IMU-838 in the mouse model of accelerated T1D, vehicle n = 14, IMU-838 n = 12.

(**H, I**) Frequencies of (**H**) $CD25^+Foxp3^+$ T cells and (**I**) of proliferating $Ki67^+CD3^+CD4^+$ T cells in the pLN and in the spleen of mice treated with the vehicle control or IMU-838 in the mouse model of accelerated T1D, vehicle n = 23, IMU-838 n = 11-12.

(**J**) Mean of the CD3 intensity in the whole pancreas quantified after immunofluorescence staining from pancreatic tissue slides from control mice or mice treated with IMU-838, vehicle n = 6, IMU-838 n = 8.

(**K**) Mean of the CD3 intensity averaged over all insulin-producing islets quantified after immunofluorescence staining from pancreatic tissue slides from control mice or mice treated with IMU-838, vehicle n = 6, IMU-838 n = 8.

(**L**) $Ki67^+CD25^+Foxp3^+$ Tregs or $Ki67^+Foxp3^-$ non-Tregs after *in vitro* Treg induction in the presence of the proinflammatory cytokines IL-6, IFN-γ and IL-1β and using naïve T cells isolated from LN of NOD mice with or without IMU-838, represented here as % of vehicle, n = 25.

Cell count of (**M**) $CD25^-Foxp3^-$ non-Tregs and (**N**) $CD25^+Foxp3^+$ Tregs in pLN of control or IMU-838-teated mice, vehicle n = 21, IMU-838 n = 15.

(**O**) Representative FACS plot and quantification for Foxp3 expression in sorted $CD4^+CD25^-CD62L^+TCRV\beta4^+$ T cells from NOD BDC2.5 mice, n = 7.

Frequency of (**P**) PD1 and (**Q**) CTLA-4 in Tregs isolated from spleen of control or IMU-838-treated mice, vehicle n = 14, IMU-838 n = 11.

Each data point represents one subject, (A-E, G-K) experiments were performed in up to seven independent experiments, (F) experiments were performed in 2-3 technical replicates. Student's *t* test. *=p<0.01; **=p<0.01.

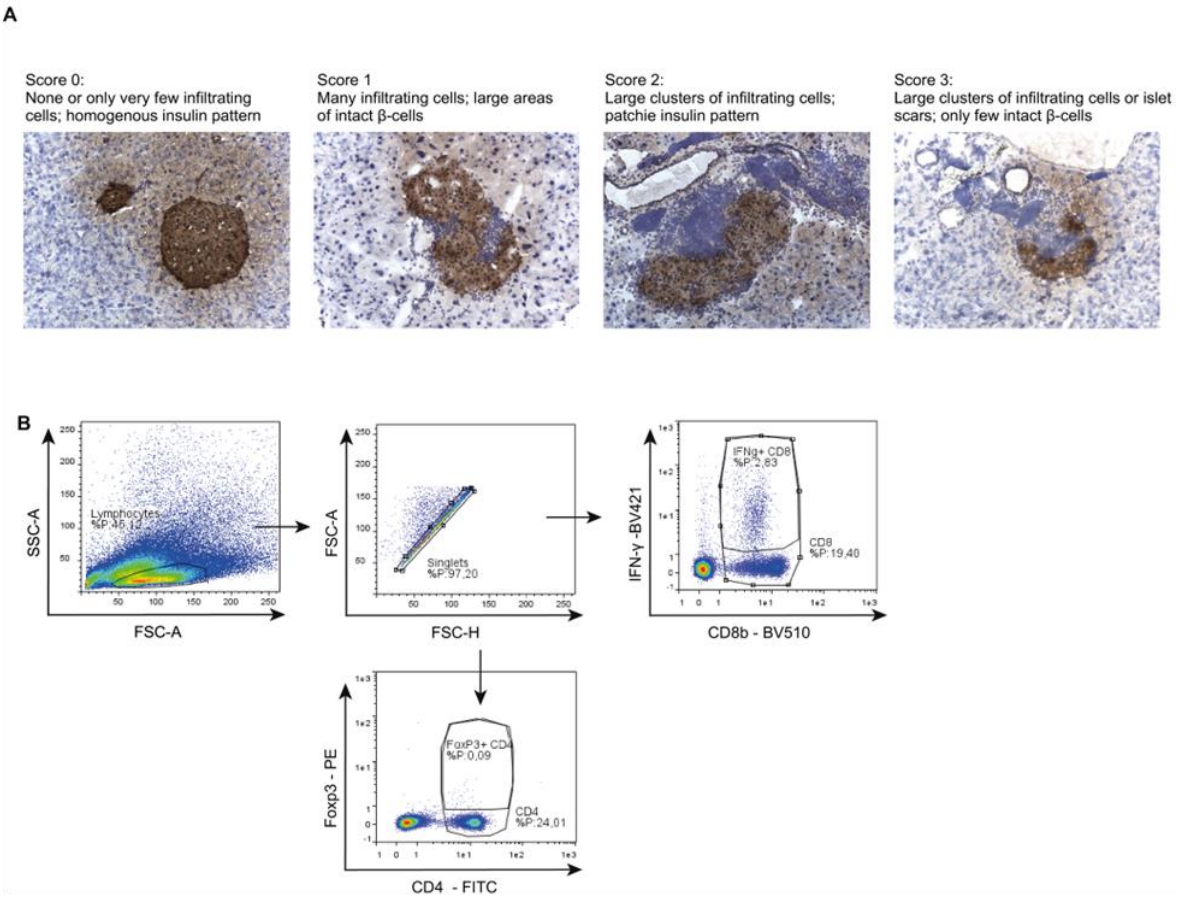

Fig. S10. Analysis of IMU-838 treatment in the virus-induced T1D RIP-LCMV-GP mouse model.

(**A**) Representative images of insulin, CD8 and hematoxylin-staining of pancreas cryosections. To evaluate the insulitis score.

(**B**) Representative FACS plots for the analysis of GP33-specific IFNγ^{+}CD8^{+} T cells and Foxp3^{+}CD4^{+} Tregs.

Table S1.

List of primers

Gene	Forward (5'-3')	Reverse (5'-3')
Histone H3	ACTGGCTACAAAAGCCG	ACTTGCCTCCTGCAAAGCAC
TCRVβ4 transgene	CATGTTTCCCTGCACATC	CCAGATCCAAAGATGAGTTGC
Rorc	GGGTGCAAGGGCTTCTTCC	CTGCTTCTTGGACATTCGGC
Dhodh	AAGATTGCCCCTGACCTCAC	GATGATGGGAATCGTGCCTTG

Table S2. Flow Cytometry Antibodies Anti-Mouse

antibody (anti-mouse)	clone	fluorophore	source
CD11b	M1/70	PB	BioLegend
CD11c	N418	BV (Brilliant Violet) 421	BioLegend
CD14	rmC5-3	V450	BD Bioscience
CD25	PC61	PerCP-Cy5.5, BV785	BioLegend
CD28	37.51	Purified	BD Bioscience
CD3	145-2C11	BV711, PE-Texas Red Purified	BioLegend BD Bioscience
CD4	GK1.5 GK 1.5 RM4-5 RM4-5	Biotin FITC Alexa Fluor 700, PE-Cy7	BioLegend Southern Biotech BD Bioscience
CD44	IM7	PE APC-Cy7	BioLegend eBioscience/Invitrogen
CD45R/B220	RA3-6B2	PB	BioLegend
CTLA-4	UC10-4B9	PerCP-Cy5.5	Biolegend
CD62L	MEL-14	BV510, APC, PE-Cy7, BV711	BioLegend
CD8a	53-6.7	PB	BioLegend
F4/80	CI:A3-1	PB	BioLegend
Foxp3	FJK-16S	FITC, PE	Invitrogen
IFN-γ	XMG1.2	Alexa Fluor 647	BioLegend
IL-10	JES5-16E3	PE	Biolegend
IL-17A	TC11-18H10.1	BV605	Biolegend
Isotype control Rat IgG2a, κ	RTK2758	PE	Biolegend
Ki67	16A8	BV605, APC	Biolegend
PD-1	29F.1A12	PE	Biolegend
RORγt	AFKJS-9	PE	eBioscience/Invitrogen
TCRVβ4	KT4	FITC	BD Pharmingen
Strep		PB	Invitrogen

Table S3.

Flow cytometry anti-human antibodies

antibody (anti-human)	clone	fluorophore	source
CD11B	ICRF44	PB	BioLegend
CD14	HCD14	PB	BioLegend
CD19	HIB19	PB	BioLegend
CD127	A019D5	PE-Cy7	BioLegend
CD25	2A3 M-A251	APC PE	BD Bioscience BD Bioscience
CD28	28.2	Purified	BioLegend
CD3	UCHT1 HIT3a	Purified, BV421 PerCp-Cy5.5	BioLegend
CD4	RPA-T4 RPA-T4 OKT4	V500 BV421 BV785	BD Horizon BD Bioscience BioLegend
CD45RA	HI100 ALB11	FITC, AF700, BV650 FITC	BioLegend Beckman Coulter
CD45RO	UCHL1	APC-Cy7 PE-Cy7	BD Pharmingen BioLegend/BD Bioscience
CD8A	RPAT8 SK-1	PB AF700	BioLegend BioLegend
FOXP3	PCH101 236A/E7	FITC PE	eBioscience/Invitrogen
KI67	16A8	BV605	Biolegend
IFNγ	4S.B3	PerCp-Cy5.5	Biolegend
IL-10	JES3-9D7	AF488	eBioscience
LAG3	11C3C65	BV711	Biolegend
TCRVβ17	IM2048	PE	Beckman Coulter